www.czasopisma.pan.pl PAN POLSKA AKADEMIA NAUK www.journals.pan.pl

Arch. Metall. Mater. **65** (2020), 2, 727-734

DOI: 10.24425/amm.2020.132812

R. KAWULOK[1*], I. SCHINDLER[1], H. NAVRÁTIL[1], V. ŠEVČÁK[1], J. SOJKA[1], K. KONEČNÁ[1], B. CHMIEL[2]

HOT FORMABILITY OF HEAT-RESISTANT STAINLESS STEEL X15CrNiSi 20-12

High-temperature plastic properties of heat-resistant stainless steel X15CrNiSi 20-12 were assessed on the basis of hot tensile tests and nil strength tests. The results were supported by metallographic analyses using SEM and EDX analysis. The formability of the investigated steel can be divided into roughly three temperature areas. In the temperature range of 900°C to about 1050°C, formability was negatively affected by precipitation of carbide particles at grain boundaries. As the temperature rose to 1200°C, these particles dissolved, resulting in an increase in formability. Further temperature increases resulted in a relatively steep drop in formability caused by overheating of the material. The nil ductility temperature of 1280°C and the nil-strength temperature of 1362°C were determined. The Plastic and strength properties of the investigated material were compared with the deformation behavior of the reference steel X5CrNi 18-10, which shows a significantly wider range of suitable forming temperatures.

Keywords: Heat-resistant stainless steel, Hot tension test, Nil strength temperature, Nil ductility temperature

1. Introduction

Austenitic heat-resistant steels had been developed on the basis of stainless steels by the end of the 19th century and today, they are widely used in construction materials for applications such as boilers, reactors, heaters, heat exchangers, etc. Their main advantage is the combination of relatively high strength, creep, oxidation and corrosion resistance and relatively low production costs [1-7]. Complications in these steels are associated with deterioration of mechanical properties and formability due to precipitation. Under operating conditions, various secondary phases can be formed in austenitic steels, such as MX carbonitrides, $M_{23}C_6$ carbides, Z phases, sigma phases, and Laves phases, which may agglomerate further due to aging [1,8-11]. Thus, the microstructure of heat-resistant steels is formed by austenitic grains, which are lined with precipitates formed in the temperature range of about 600-1000 (1050)°C. These particles lead to embrittlement, and the steel is subjected to dissolution annealing, which usually takes place in the range of 1000-1100°C. Another negative effect is the reduced recrystallization ability of austenitic heat-resistant steels [12-18].

MX carbonitrides and $M_{23}C_6$ type carbides have an fcc lattice and normally nucleate further along the grain boundaries and in locations with higher dislocation density. This phenomenon is associated with the rate of diffusion, which is higher in these places than in the remaining volume [19-24]. The $M_{23}C_6$ carbide roughening rate is much higher than that of MX type carbonitrides, which promotes high temperature creep. Microalloying elements, such as Ti, Nb and V also contribute to the formation of MX carbonitirides, and since they have a higher carbon affinity than chromium, they are used to reduce and slow down the formation of $M_{23}C_6$ carbides. $M_{23}C_6$ carbides posited along the grain boundaries can also cause inter-crystalline corrosion [22-24].

The aim of the work was to evaluate the hot formability of chromium nickel austenitic stainless steel and heat-resistant X15CrNiSi 20-12. This steel is used for the construction of heat treatment equipment, parts of boilers and furnace aggregates (fittings, grates, conveyors, hinges), heat exchanger and fan components, for thermally stressed parts of ceramic and glass furnaces, thermocouple protective sleeves, as heat stressed fasteners and others [1,2]. The deformation behavior study will be based mainly on uniaxial hot tensile tests, a very sensitive method due to the prevailing tensile components of the stress in formability evaluation. The parameters evaluated are ductility, contraction and ultimate tensile strength. The tensile test results can be used to determine the NDT (Nil ductility temperature) at which the formability of the material is exhausted and fracture

[1] VSB – TECHNICAL UNIVERSITY OF OSTRAVA, FACULTY OF MATERIALS SCIENCE AND TECHNOLOGY, 17. LISTOPADU 15/2172, 708 00 OSTRAVA – PORUBA, CZECH REPUBLIC
[2] TŘINECKÉ ŽELEZÁRNY, A.S., PRŮMYSLOVÁ 1000, 739 61 TŘINEC, CZECH REPUBLIC

* Corresponding author: rostislav.kawulok@vsb.cz

occurs under load without evidence of elongation of the test specimen. Another critical temperature for the high temperature region of metallic materials is the nil strength temperature (NST) at which the material loses all its strength during heating due to the grain boundary melting, i.e.temperature at which the material does not tolerate any load. NST is always higher than NDT, but both of these critical temperatures are highly dependent on the chemical composition of the material [12,25-27].

2. Experimental

Steel X15CrNiSi 20-12 with chemical compositionin Table 1 was supplied in a post-hot rolling condition.

TABLE 1

Chemical composition of X15CrNiSi 20-12 steel in wt.%

X15CrNiSi 20-12	C	Mn	Si	Cr	Ni	Mo	N
	0.16	1.01	1.54	20.2	12.3	0.27	0.07

The deformation behavior was investigated on a hot deformation simulator Gleeble 3800. Tests for determining the nil-strength temperature (NST) were performed on cylindrical samples with a diameter of 6 mm and a length of 81 mm. These samples were loaded with a constant tensile force of 80 kN throughout the test via air controlled piston. At the same time, the resistive heating of the samples was carried out at a rate of 20°C·s^{-1} up to a temperature 1200°C, and then the heating was slowed down to 2°C·s^{-1}, while the temperature was linearly increasing to the fracture of the sample caused by the combination of melting effect grain boundaries and very low tensile forces. In order to eliminate the effect of possible inhomogeneities in the investigated materials and also for statistical evaluation, this test was repeated 3 times – see Fig. 1. The average NST was 1362°C with a relatively low standard deviation of ±4°C.

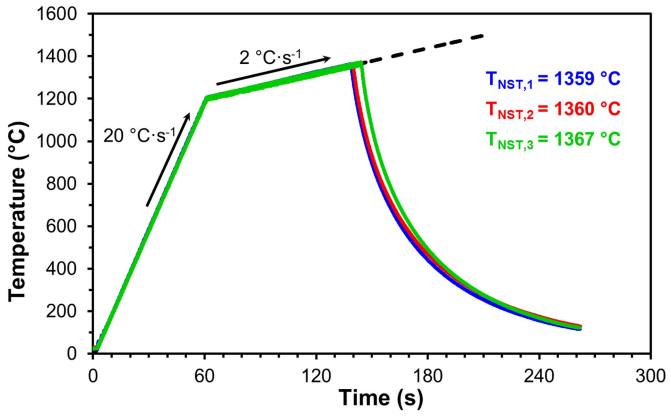

Fig. 1. Records of NST measurement for steel X15CrNiSi 20-12

For hot tensile testing, cylindrical specimens with a diameter of 10 mm and a length of 116.5 mm were prepared and threaded on the end portions. Hot-grips stainless steel jaws (Fig. 2) were used for uniaxial tension tests, which are used to provide uniform heating in the 20 mm zone [25,26]. Tensile tests were carried out in the temperature range of 900-1280°C. The resistance heating of the samples was at the rate of 10°C·s^{-1} directly to the deformation temperature, where 180 s delay followed. The pull of the sample into the fracture was at a stroke rate of 50 mm·s^{-1}.

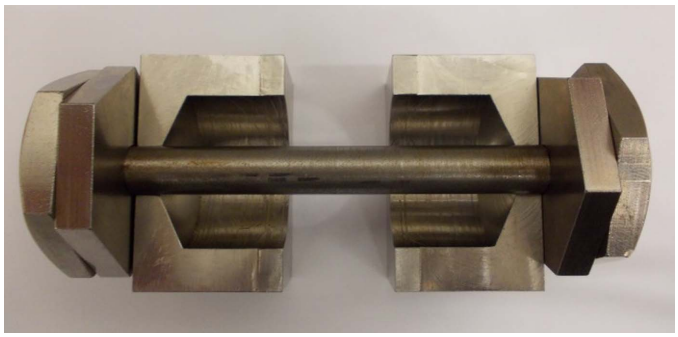

Fig. 2. Placement of samples in hot grips jaw type for tests on simulator Gleeble 3800

Tensile diagrams (see Fig. 3) from which the maximum force values F_{max} (kN) and the sample elongation till fracture ΔL (mm) were determined. These values were subsequently used to calculate the ultimate tensile strength R_mT (MPa) and the hot ductility A_T (%):

$$R_{mT} = \frac{F_{max} \cdot 1000}{S_0} \tag{1}$$

$$A_T = \frac{\Delta L}{L_0} \cdot 100 \tag{2}$$

Where ΔL is elongation till fracture (mm) and $L_0 = 20$ mm is the initial measured length.

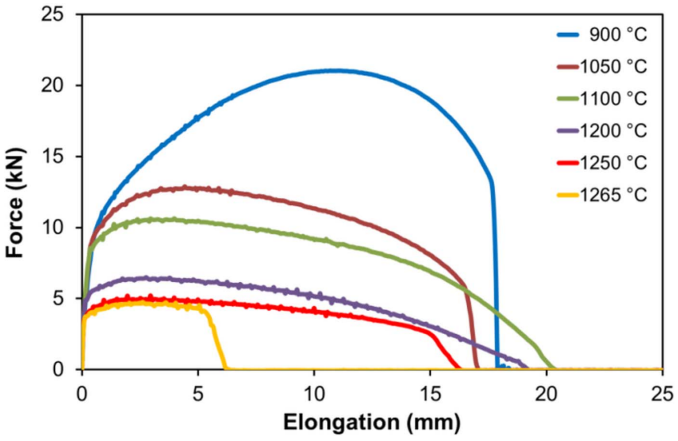

Fig. 3. Graphical representation of the hot tensile test of steel X15CrNiSi 20-12

Contraction Z_T (%) was expressed by cross-sectional areas of test bars after breaking S_1 (mm^2) and initial cross-section $S_0 = 78.5$ mm^2:

$$Z_T = \frac{S_0 - S_1}{S_0} \cdot 100 \qquad (3)$$

Selected samples were subjected to metallographical analyses (light microscopy, SEM and EDX). Conventional metallographic examination by light microscopy was used for the microstructure analysis. Polishing and grinding was done by using papers and SiO_2 suspensions. The grain size calculation was based on the intercept lengths measurement using the software Quick PHOTO INDUSTRIAL 3.2. For a sample heated to 1050°C, supplementary analysis of the precipitates was performed by the SEM method on a JEOL JSM-6490LV scanning electron microscope equipped with an INCA x-act energy dispersion analyzer (Oxford Instruments). Chemical etching was realized with a reagent of 10 parts H_2O, 10 parts HNO_3 and 1 part HCl.

For comparison, analogous experiments were performed on reference austenitic stainless steel X5CrNi 18-10, the chemical composition of which is given in Table 2.

TABLE 2

Chemical composition of X5CrNi 18-10 steel in wt.%

	C	Mn	Si	Cr	Ni	Mo	N
X5CrNi 18-10	0.024	1.55	0.37	18.2	8.0	0.25	0.07

3. Results and discussion

Hot deformation behavior of steel X15CrNiSi 20-12

Examples of broken samples are shown in Fig. 4. Fig. 5 shows the fracture surfaces for the selected two forming temperatures. In the case of 1280°C, the significant coarsening of the grain, which has a mean size of about 0.4 mm, is clearly visible. Significant coarsening of the grain is probably due to a combination of several causes. Significant coarsening of the grain tends to be associated with the presence of anchored structure due to particles of other phases or a larger size of the primar grain, including other crystallographic orientation.

As can be seen from Fig. 3, with increasing temperature, the contract strength decreases to a temperature of about 1265°C.

Fig. 4. Selected examples of samples after test

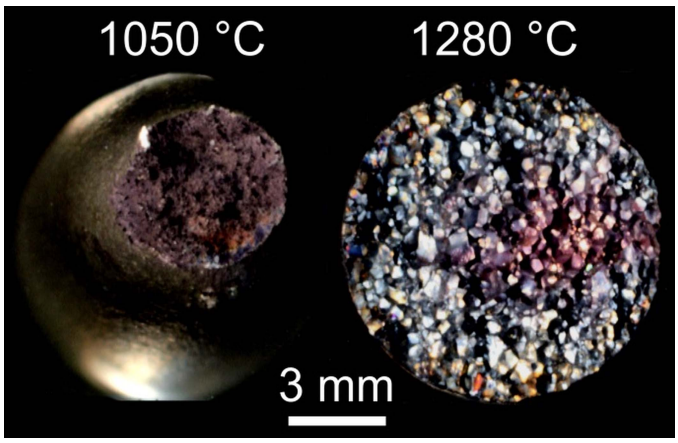

Fig. 5. Examples of fracture surfaces after sample failure

This phenomenon is displayed along with the ductility dependence on deformation temperature in Fig. 6. It is also evident from this graph that the highest formability can be expected for the investigated steel within a narrow temperature range of about 1100 to 1200°C, which is in agreement with authors [2,14]. When the temperature was increased further, the formability dropped sharply, with an NDT of 1280°C being determined.

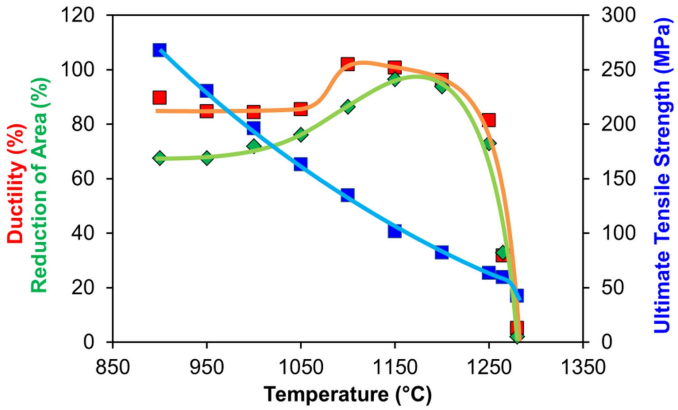

Fig. 6. Thermal dependence of ductility till fracture, contraction and ultimate tensile strength steel X15CrNiSi 20-12

Initial structure affected by the heating temperature of steel X15CrNiSi 20-12

The initial material structure is characterized by considerable heterogeneity with the appearance of grains of the order of tenths of a millimeter – see Fig. 7.

In order to clarify the measured data, further experiments were conducted aimed at studying the structure of the samples before deformation. Tensile samples were heated to selected temperatures of 900°C, 1050°C, 1200°C, or 1280°C, and their structure was fixed by quenching. Metallographic images of structures after heating in Fig. 8 document austenitic grains, often with characteristic twins. The original coarse grains remained at heating temperatures of 900-1050°C. Dark etching artifacts signal the occurrence of inclusions.

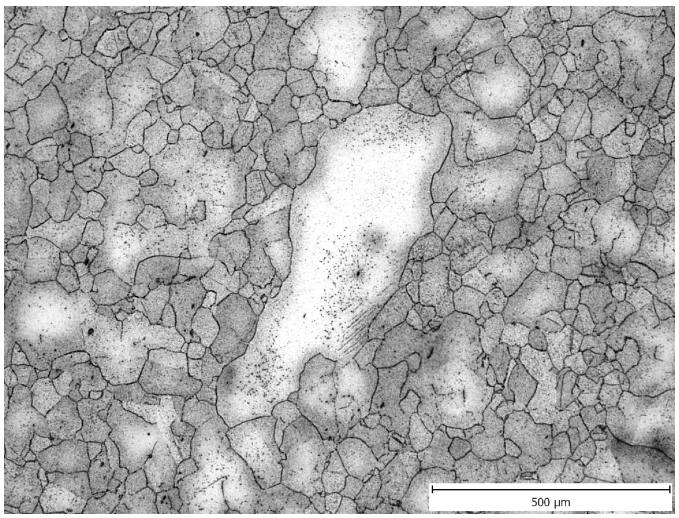

Fig. 7. Initial structure of X15CrNiSi 20-12

It has been verified that the acceleration of grain growth occurs above a temperature of about 1100°C – see Fig. 9.

In the temperature range of 900-1050°C, small formations occur in particular in the form of chains (see Fig. 10a), which are very likely to reduce formability – this corresponds to the graph in Fig. 6. At these temperatures, the grain boundary diffusion takes place much faster than in the remaining volume and grain boundaries provide preferred nucleation sites for carbide particle precipitation. At higher temperatures, these formations dissolve at the grain boundaries (see Fig. 10b) and thus increase formability. Examples of similar mechanisms are described in several papers [1,28-31].

The drop in formability at temperatures above 1200°C is mainly due to overheating of the material, which is associated with significant coarsening of the grain.

SEM/EDX analysis

Fig. 11a) illustrates the character of the backscattered electron precipitation pattern after polishing the sample. It is clear that precipitates formed near-continuous mesh at the grain boundaries, and were typically in the range of about 0.5-2.5 µm and to a small extent precipitates of up to 5 µm in length were also observed. A small portion of precipitates was also present within the austenitic grains. Fig. 11b) shows the character of precipitation after etching. To clarify the nature of the precipitates, an EDX analysis of their chemical composition was performed. Fig. 12 compares the results of EDX analysis of the metal matrix and the precipitate particles. The results of

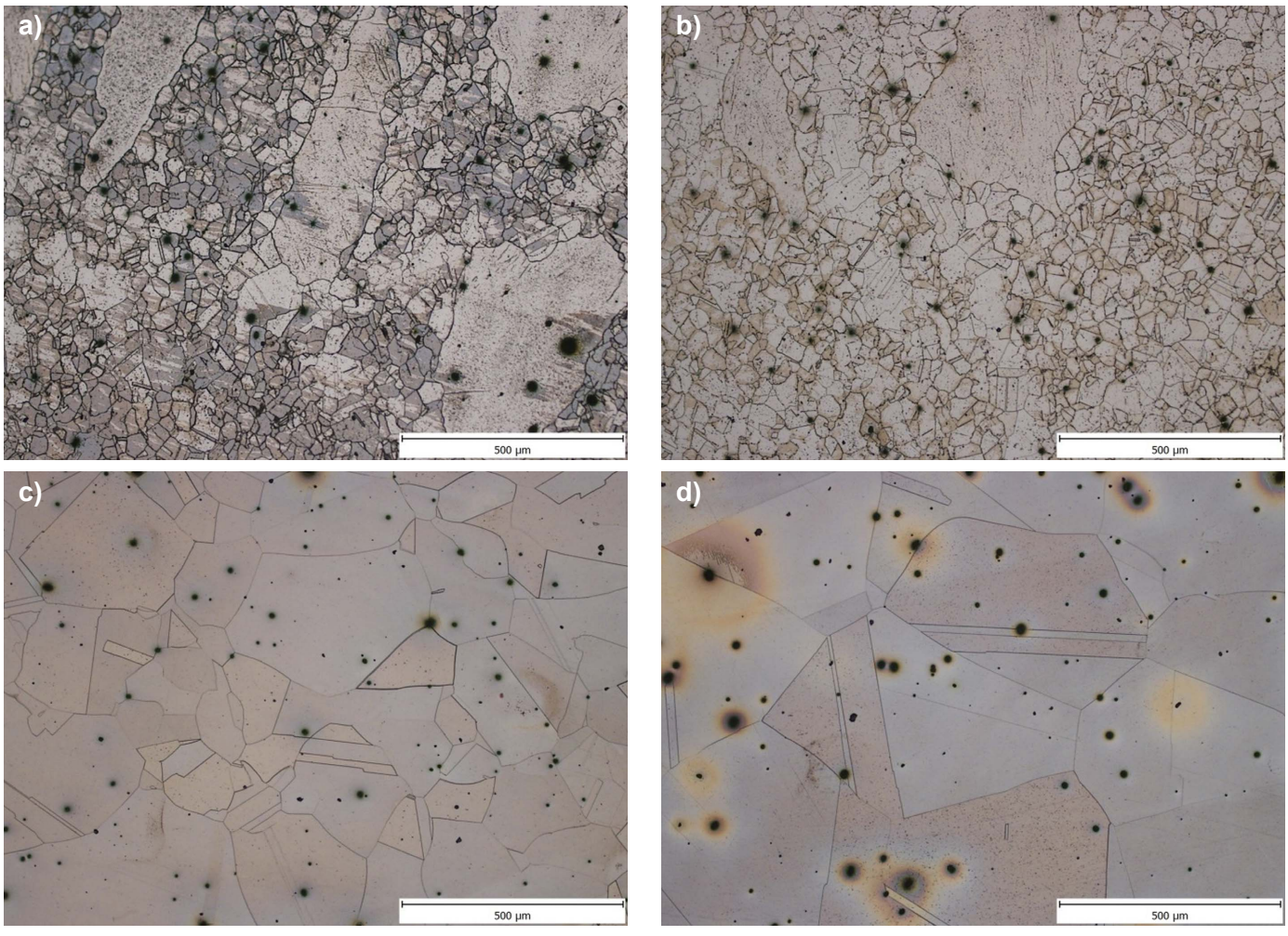

Fig. 8. Examples of the microstructure of selected heating temperatures of steel X15CrNiSi 20-12; a) 900°C, b) 1050°C, c) 1200°C, d) 1280°C

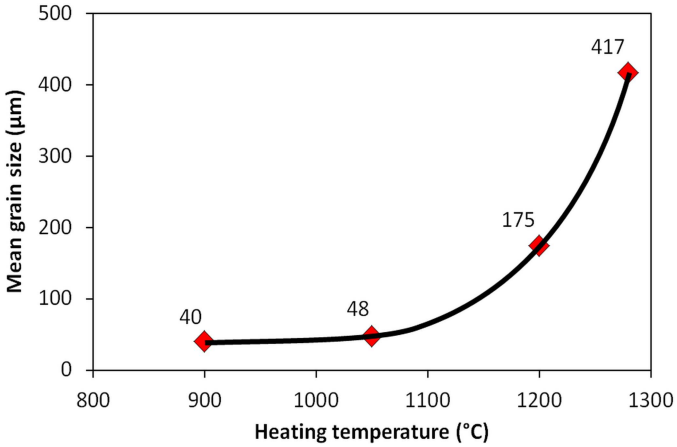

Fig. 9. Influence of heating temperature on grain size X15CrNiSi 20-12

a series of analyses showed that the precipitates are likely to be $M_{23}C_6$ type carbides containing preferably Cr but also increased the content of molybdenum (54.34% Cr; 30.48% Fe; 9.27% C; 3.48% Ni; 1.33% Mo; 0.75% Mn; 0.35% Si). The content of Si in the precipitates was always lower compared to the metal matrix (19.43% Cr; 60.73% Fe; 5.29% C; 11.51% Ni; 0.35% Mo; 1.07% Mn; 1.62% Si). The presence of $M_{23}C_6$ carbides in the sample heated to 1050°C is probably due to the fact that the increased proportion of silicon in chromium-nickel steels promotes precipitation of this type of carbide and increases the temperature range at which the carbide is stable [32]. The delay time at 1050°C was probably not sufficient to dissolve the carbide precipitates, because their formation during cooling should be eliminated due to the quenching of the sample into water. For the studied steel, the temperature of 1050°C represents the lower limit of the recommended solution annealing interval [1,2]

The same sample, EDX analysis of the chemical composition of the coarser non-metallic inclusions was also performed – see Fig. 13 and 14. Coarser non-metallic inclusions were found to be complex oxysulfides. Al_2O_3 – based oxides were present in the center of the inclusions and contained an increased Ca content (47.5% Al; 46.1% O; 5.6% Ca; 0.4% Cr; 0.4% Fe). The inclusion envelope was a sulphide of the (Mn, Ca)S type (46.7% Mn; 35.0% S; 7.5% Ca; 5.2% Cr; 2.1% Al; 2.1% O; 1.6% Fe).

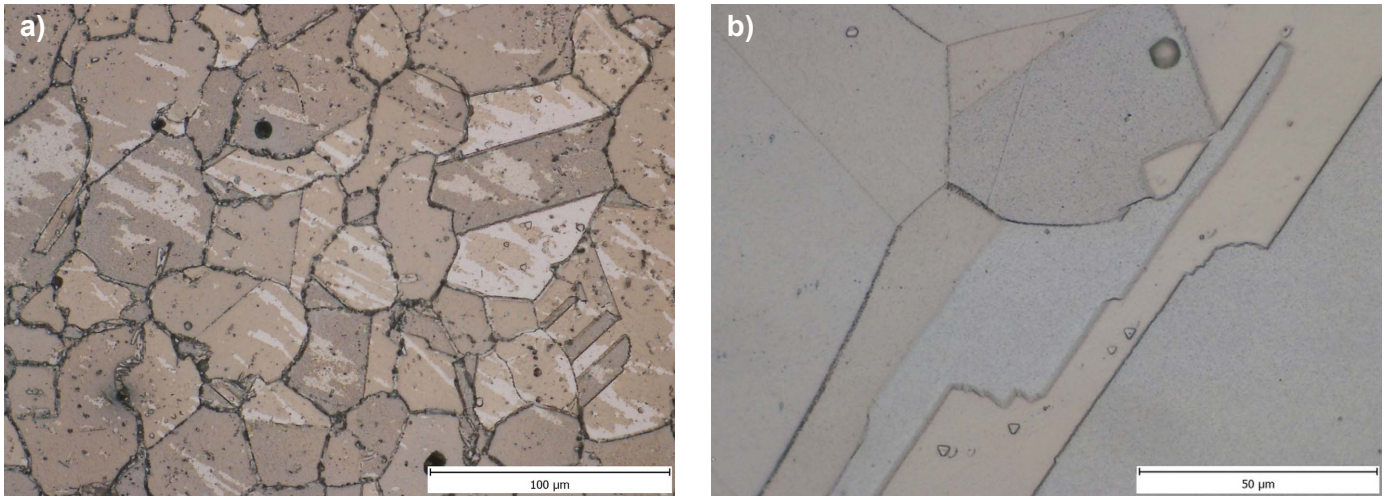

Fig. 10. Grain boundaries with and without fine elements in steel X15CrNiSi 20-12; a) 900°C, b) 1200°C

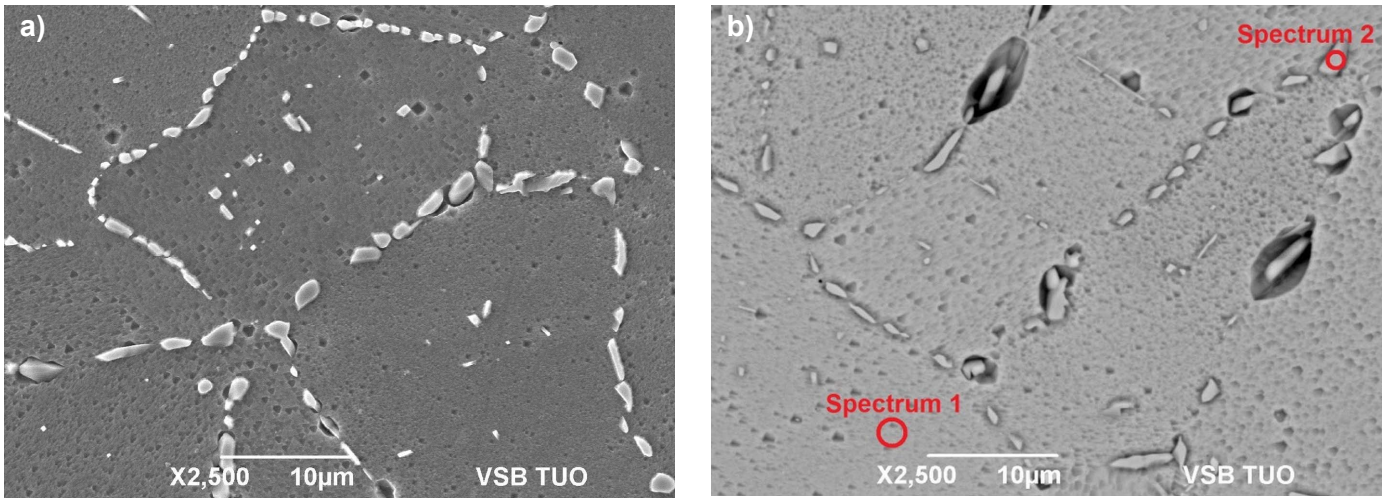

Fig. 11. SEM microscopy of sample structure with particles on grain boundaries after heating at 1050°C; a) Polished sample, b) Etched sample with local sites of chemical EDX analysis

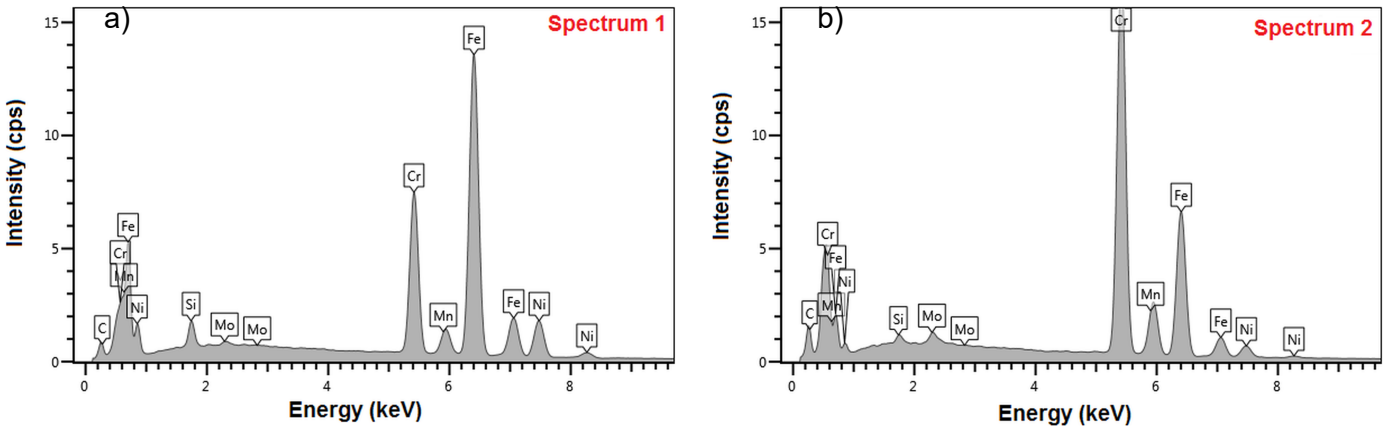

Fig. 12. EDX analysis of sample at 1050°C; a) matrix (Spectrum 1), b) precipitate (Spectrum 2)

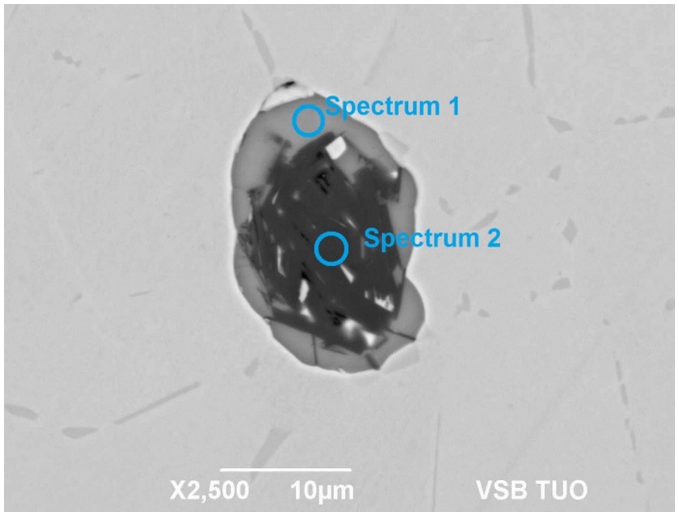

Fig. 13. Example of inclusion in sample 1050°C

of 32°C compared to steel X15CrNiSi 20-12. This corresponds to the temperature dependence of strength and formability in Fig. 16-17.

Due to the higher content of C, Cr and Si, and the expected lower recrystallization capacity, the steel X15CrNiSi 20-12 shows greater strength especially at low temperatures, the differences are negligible at the temperature range of 1200-1250°C. This effect is most likely due to the higher content of C, Cr and Si since these elements significantly affect strength and plasticity as well as recrystallization kinetics. Silicon has a similar effect to Cr in austenitic steels. The higher silicon content, which is dissolved in austenite, gradually decreases formability throughout the hot forming temperature, and this effect is particularly apparent for Si contents above 1%. Chromium in solid solution increases strength, increases activation energy and reduces recrystallization ability, especially in high alloy austenitic steels. The Formation

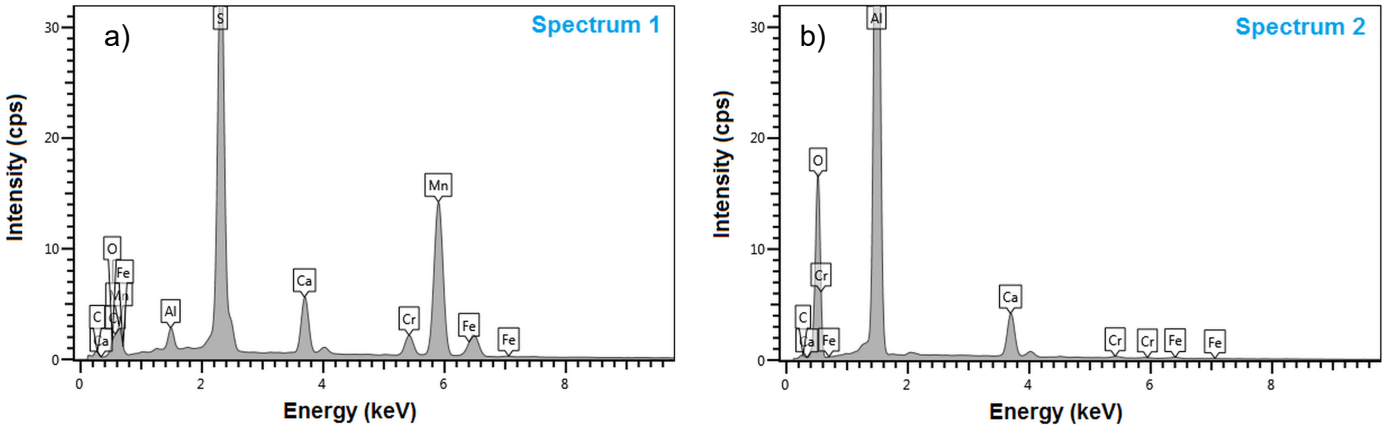

Fig. 14. EDX analysis of inclusion for the sample at 1050°C; a) Inclusion envelope formed by (Mn,Ca)S, b) The central part of the Al_2O_3-based inclusions with increased Ca content

Comparison of hot deformation behaviour of X15CrNiSi 20-12 and X5CrNi 18-10 steels

For reference steel X5CrNi 18-10, a nil-strength temperature of 1394°C was determined with a standard deviation of ±1°C (see Fig. 15), indicating a relative reduction of NST

of chromium carbide unfavorably affects formability in the lower forming temperature range. The critical deformation ε_c required for the initiation of dynamic recrystallization of austenitic types of steels is generally higher in the range 1000-850°C than $\varepsilon_c > 0.5$. In particular, dynamic recovery with partial removal of reinforcement is taking place in forming such alloyed austenitic

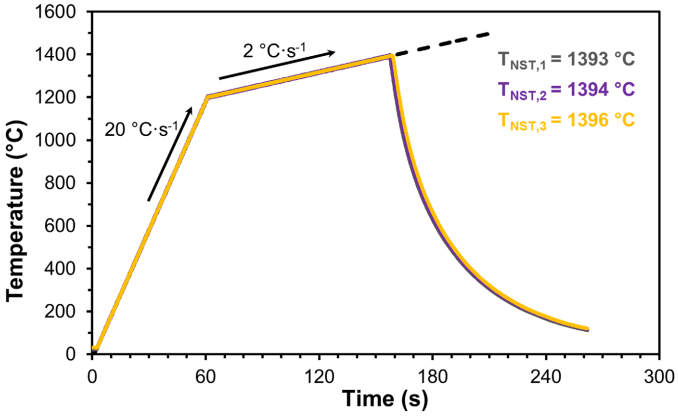

Fig. 15. Graph of NST measurement for steel X5CrNi 18-10

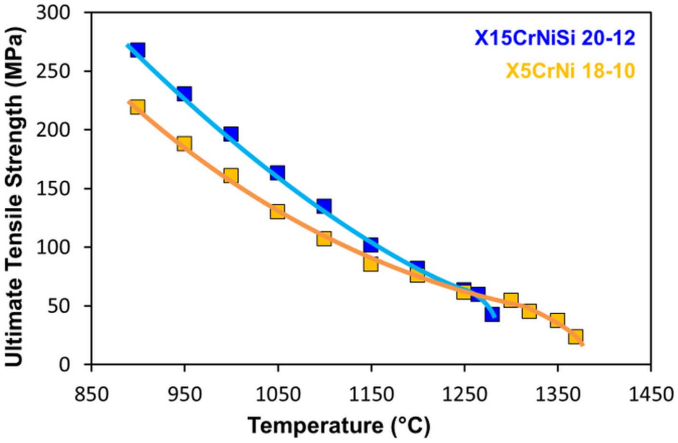

Fig. 16. Comparison of strength of two steels X15CrNiSi 20-12 and X5CrNi 18-10

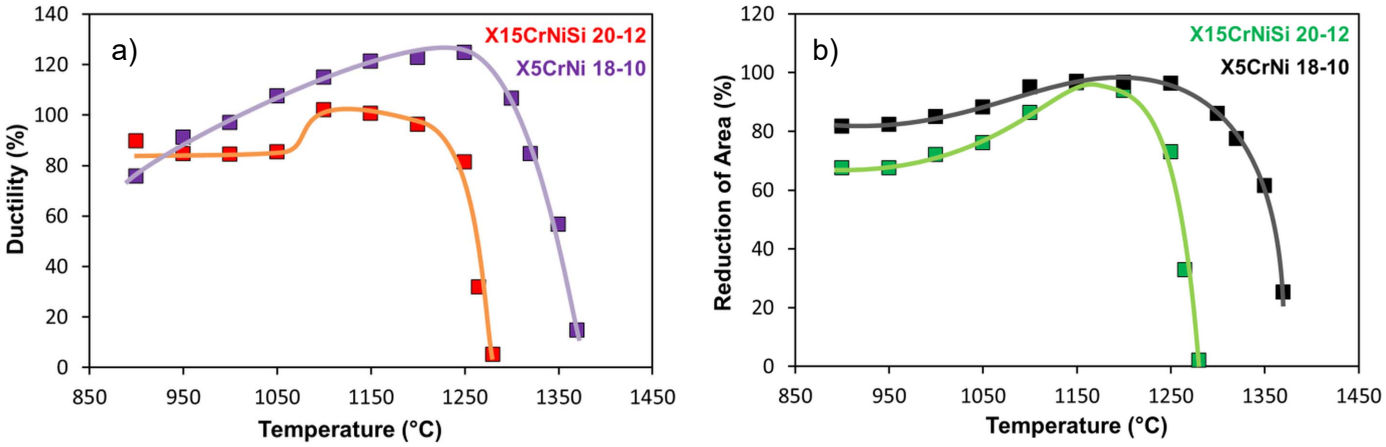

Fig. 17. Comparison of the temperature dependence of plastic properties of steels X15CrNiSi 20-12 and X5CrNi 18-10; a) Ductility, b) Reduction of area

steels, but the decisive part of recovery is due to post-dynamic processes [12-14].

Fig. 17 shows that the hot formability of X15CrNiSi 20-12 is virtually lower over the entire temperature range compared to the reference less alloyed steel. The reasons are analogous to the differences in strength.

Nil ductility temperature (NDT) has a value of approx. 1374°C for X5CrNi 18-10 steel; this is 94°C more than in the case of X15CrNiSi 20-12, which therefore shows a much narrower range of suitable forming temperatures. There is a variety of calculations for determining solidus T_S and T_L liquidus temperature values, but only a few are suitable for complex alloyed austenitic stainless steels [33-35].

The experimentally determined NDT and NST values correspond to the solidus T_S and T_L liquidus temperature calculations according to formulas [36]:

$$T_S = 1535 - 200(\%C) - 183.9(\%S) - 12.3(\%Si) - 6.8(\%Mn) - 4.3(\%Ni) - 1.4(\%Cr) - 4.1(\%Al) - 124.5(\%P) \quad (41)$$

$$T_L = 1537 - 88(\%C) - 25(\%S) - 5(\%Cu) - 8(\%Si) - 5(\%Mn) - 2(\%Mo) - 4(\%Ni) - 1.5(\%Cr) - 18(\%Ti) - 2(\%V) - 30(\%P) \quad (4)$$

A comparison of all critical temperatures for the high temperature region of the two investigated steels is given in Table 3.

TABLE 3

Critical temperatures of investigated steels

	NDT (°C)	NST (°C)	T_S (°C) [36]	T_L (°C) [36]
X15CrNiSi 20-12	1280	1362	1387	1423
X5CrNi 18-10	1374	1394	1448	1463

The difference in NST and NDT values should be around 30°C with a tolerance of ±15°C, according to the authors of the papers [26,27]. This corresponds to a difference of 20°C in the case of steel X5CrNi 18-10, but the difference of 82°C in steel X15CrNiSi 20-12 is abnormally large and confirms the unsuitability of applying high forming temperatures.

4. Conclusions

Critical temperatures associated with high temperature plasticity of heat-resistant stainless steel X15CrNiSi 20-12 was found, i.e. NDT = 1280°C and NST = 1362°C. It has been found that the temperature range most suitable for forming this steel has a very narrow range of 1100-1200°C. At lower temperatures, the formability is slightly reduced due to the fine carbide mesh along the grain boundaries, mainly formed by $M_{23}C_6$ particles. As the temperature rises up to about 1200°C, these particles dissolve, resulting in improved plastic properties. The relatively steep drop in formability at temperatures above 1200°C is mainly due to grain growth in connection with material overheating.

A comparison of the deformation behavior of the investigated steel with austenitic stainless steel X5CrNi 18-10 showed that the alloy with lower C, Cr and Si content showed lower strength and formability at virtually all temperatures above 900°C. At the same time, the reference NDT and NST values of the reference steel are significantly higher than in the case of X15CrNiSi 20-12.

Acknowledgements

This paper was created at the Faculty of Materials Science and Technology within the Project No. CZ.02.1.01/0.0/0.0/17_049/0008399 funded by the Ministry of Education, Youth and Sports of the Czech Republic; and within the students' grant project SP2020/88 supported at the VŠB – TU Ostrava by the Ministry of Education of the Czech Republic.

REFERENCES

[1] Y. Zhou, Y. Liu, X. Zhou, C. Liu, J. Yu, Y. Huang, H. Li, W. Li, J. Mater. Sci. Technol. **33**, 1448-1456 (2017).

[2] J.A. Lichtenfeld, M.C. Mataya, Ch.J. Van Tyne, Metall. Mater. Trans. A **37A**, 147-161 (2006).

[3] M.S. Ghazani, B. Eghbali, Mater. Sci. Eng. A **730**, 380-390 (2018).

[4] J. Fu, J. Sun, X. Cen, X. Zhang, F. Li, Y. Wu, Mater. Charact. **139**, 241-248 (2018).

[5] V.A. Hosseini, L. Karlsson, D. Engelberg, S. Wessman, Weld. World. **62**, 517-533 (2018).

[6] R.K.C. Nkhoma, C.W. Siyasiya, W.E. Stumpf, J. Alloys Compd. **595**, 103-112 (2014).

[7] R.V. Taiwade, R. Shukla, H. Vashishtha, A.V. Ingle, R.K. Dayal, ISIJ Int. **53** (12), 2206-2212 (2013).

[8] J. Man, M. Smaga, I. Kuběna, D. Eifler, J. Polák, Eng. Fract. Mech. **185**, 139-159 (2017).

[9] W.H. Kan, V. Bhatia, K. Dolman, T. Lucey, X. Tang, L. Chang, G. Proust, J. Cairney, Wear. **389-399**, 220-226 (2018).

[10] D. Iacoviello, F. Iacoviello, M. Macario, La Metallurgia Italiana. **25** (3), 1-6 (2003).

[11] M. Aghaie-Khafri, F. Honarvar, S. Zanganeh, J. Nondestruct. Eval. **31** (3), 191-196 (2012).

[12] M. Žídek, Metalurgická tvařitelnost ocelí za tepla a za studena, ALEKO, Prague (1995).

[13] R. Baron, R. Fabík, in: Metal 2011, Ostrava: Tanger Ltd, paper no. 951 (2011).

[14] P. Turoňová, I. Schindler, P. Jonšta, M. Heger, J. Bořuta, L. Černý, in: Metal 2005, Ostrava: Tanger Ltd, paper no. 63 (2005).

[15] L. Duprez, B.D. Cooman, N. Akdut, Steel Res. **71** (10), 417-422 (2000).

[16] H. Sun, Y. Sun, R. Zhang, M. Wang, R. Tang, Z. Zhou, Mater. Des. **64**, 374-380 (2014).

[17] M. Schymura, R. Stegemann, A. Fischer, Int. J. Fatigue. **79**, 25-35 (2015).

[18] A. Moteshakker, I. Danaee, J. Mater. Sci. Technol. **32** (3), 282-290 (2016).

[19] M. Vach, T. Kuníková, M. Dománková, P. Ševc, L'. Čaplovič, P. Gogola, J. Janovec, Mater. Charact. **59** (12), 1792-1798 (2008).

[20] S. Das, M. Mukherjee, T.K. Pal, Eng. Failure Anal. **54**, 90-102 (2015).

[21] C. Hutchinson, H. Zurob, C. Sinclair, Y. Brechet, Scr. Mater. **59** (6), 635-637 (2008).

[22] O. Yoo, Y.J. Oh, B.S. Lee, S.W. Nam, Mater. Sci. Eng. A. **405** (1-2), 147-157 (2005).

[23] W.M. Rainforth, M.P. Black, R.L. Higginson, E.J. Palmiere, C.M. Sellars, I. Prabst, P. Warbichler, F. Hofer, Acta Mater. **50** (4), 735-747 (2002).

[24] S. Jin, L. Guo, F. Luo, Z. Yao, S. Ma, R. Tang, Scr. Mater. **68** (2), 138-141 (2013).

[25] P. Kawulok, I. Schindler, R. Kawulok, S. Rusz, P. Opěla, J. Kliber, M. Kawuloková, Z. Solowski, K.M. Čmiel, Metalurgija. **55** (3), 365-368 (2016).

[26] I. Schindler, R. Mendrok, P. Kawulok, P. Unucka, R. Kawulok, P. Opěla, S. Rusz, R. Turoň, P. Turoňová, A. Bořuta, in: Metal 2014, Ostrava: Tanger Ltd, paper no. 2504 (2014).

[27] A. Mertová, P. Kawulok, I. Schindler, B. Smetana, S. Zlá, R. Kawulok, S. Rusz, P. Opěla, Ľ. Drozdová, V. Ševčák, Hutnické Listy **70** (6), 11-18 (2017).

[28] A.F. Candelária, C.E. Pinedo, J. Mater. Sci. Lett. **22**, 1151-1153 (2003).

[29] X. Tao, J. Gu, L. Han, ISIJ Int. **54** (7), 1705-1714 (2014).

[30] M.W.A. Rashid, M. Gakim, Z.M. Rosli, M.A. Azam, Int. J. Electrochem. Sci. **7**, 9465-9477 (2012).

[31] L.N. Bartlett, D.C. Van Aken, J. Medvedeva, D. Isheim, N.I. Medevedeva, K. Song, Metall. Mater. Trans. A. **45A**, 2421-2435 (2014).

[32] H.S. Khatak, B. Raj, Corrosion of Austenitic Stainless Steels; Mechanism, Mitigation and Monitoring. Cambridge: Woodhead Publishing Limited, 2002.

[33] O. Martiník, B. Smetana, J. Dobrovská, S. Zlá, M. Kawuloková, K. Gryc, Ľ. Drozdová, P. Dostál, B. Martiníková, J. Phase Equilib. Diffus. **40** (1), 93-103 (2019).

[34] J. Miettinen, A.A. Howe, Ironmaking Steelmaking. **27** (3), 212-227 (2000).

[35] E. Kivineva, N. Suutala, Ruostumattomien terästen likviduslämötilojen riippuvuus koostumukseta, Report 5397-109/87, Outokumpu Oy, Tornio, Finland, 1987.

[36] J.M. Cabrera-Marrero, V. Carreno-Galindo, R.D. Morales, F. Chavez-Alcala, ISIJ Int. **38** (8), 812-821 (1998).